Journal of Materials Science: Materials in Electronics
https://doi.org/10.1007/s10854-020-03550-0

Synthesis and characterization of platinum multi-walled carbon nanotubes nanocomposite film electrode

S. O. Ibrahim[1] · K. U. Isah[1] · A. S. Abdulkareem[2] · U. Ahmadu[1] · J. O. Tijani[3] · W. D. Roos[4]

Received: 27 November 2019 / Accepted: 6 May 2020

Abstract
Carbon nanotubes (CNTs) were synthesized by a bimetallic (Fe–Co/$CaCO_3$) catalytic chemical vapour deposition (CCVD) method. The synthesized CNTs were purified with acid to remove the catalyst impurities to enhance the deposition of platinum (Pt) onto the CNTs surface. Platinum multiwall (Pt-MWCNTs) nanocomposites were produced by a wet impregnation technique dispersed in Texanol and Acrylic resins to form a paste. The paste was screen printed on an FTO glass substrate. Surface morphology, microstructure, chemical composition, crystallographic phase, surface area and electrical performance of the Pt-MWCNTs nanocomposites were measured by HRSEM, HRTEM, EDS, XPS and XRD. The electrical conductivity of the electrode produced was found to be 4.927 S m^{-1}. The results showed that the prepared nanocomposites will be a good electrode material in solar cell applications.

1 Introduction

CNTs are extraordinary nanostructured materials with distinct hexagonal tubular structures and large aspect (length/diameter) ratios. They are widely utilized in the field of material science for diverse applications such as water purification, hydrogen storage, reinforced composites, electrodes for fuel cells and solar cells, and numerous other applications [1, 2]. Carbon nanotubes have been prepared using a number of laboratorial and industrial methods (techniques) such as Arc-discharge technique [3–6], Laser-ablation technique [7–9], Flame synthesis method [10, 11], Solar method [12, 13] and Chemical vapour deposition (CVD) technique [14–16]. Nowadays, attention has been focused on the utilization of CVD technique for the synthesis of carbon nanotubes due to the following advantages over other techniques: readily availability of materials, simple reaction conditions, and easy to control, cheap in terms of unit price and can be used for continuous operation which make it suitable for large industrial process. Scientists are interested in nanotubes due to the relatively easy modifications to the tubes, which alter the surface chemistry/structure leading to novel and prospective applications. Therefore, it is important to investigate the effects of decorating carbon nanotubes (CNTs) surfaces with metal and semiconductor nanoparticles (NPs). Nanocomposite obtained through this process is expected to be a valued material owing to the combination of unique physical and chemical properties of the components.

Platinum (Pt) has attracted much attention because of its excellent catalytic activity especially in fuel cell technology [17]. Pt also remains the most stable electrode material in solar cells [18, 19]. Despite these recognitions, the cost of Pt remains a major challenge for its application in solar cell development. To resolve this problem, the use of CNTs as a

✉ S. O. Ibrahim
sharifat.ibr@futminna.edu.ng

K. U. Isah
kasim309@futminna.edu.ng

A. S. Abdulkareem
kasaka2003@futminna.edu.ng

U. Ahmadu
umaruahmadu@futminna.edu.ng

J. O. Tijani
jimohtijani@futminna.edu.ng

W. D. Roos
rooswd@ufs.ac.za

[1] Department of Physics, Federal University of Technology, PMB 65, Minna, Nigeria

[2] Department of Chemical Engineering, Federal University of Technology, PMB 65, Minna, Nigeria

[3] Department of Chemistry, Federal University of Technology, PMB 65, Minna, Nigeria

[4] Department of Physics, University of The Free State, P.O. Box 339, ZA-9300 Bloemfontein, Republic of South Africa

Published online: 11 May 2020

support, will drastically reduce the quantities of Pt required Padmavathi et al. [20] prepared Pt-MWCNTs by reduction of chloroplatinic acid to Pt and subsequently deposit Pt particles on commercial multi-walled carbon nanotubes under different reaction time. The author revealed that the prepared Pt-MWCNTs could be suitable for proton exchange membraned fuel cells. Bharti et al. [21] also employed both microwave assisted and chemical reduction methods to prepared Pt-MWCNTs catalyst for proton exchange membrane fuel cell application. The author found that small quantity of uniformly distributed platinum nanoparticles on the CNTs was better achieved using microwave assisted method than modified chemical reduction method.

This study report for the first time the development of a Pt-MWCNT composite for electrode application. Bimetallic Fe–Co/$CaCO_3$ catalyst was used to synthesize multi-walled carbon nanotubes (MWCNTs) via a catalytic chemical vapour deposition (CCVD) method. This was followed by deposition of platinum nanoparticles on the surface of the CNTs. The effect of deposition time on the quantity of platinum deposited was investigated. The electrical conductivity was estimated using a Screen-Printing Technique (SPT) onto a Fluorine-doped Tin Oxide (FTO) glass substrate. The samples were characterized using the following analytical techniques; UV–VIS Spectroscopy, High Resolution Scanning Electron Microscopy (HRSEM), High Resolution Transmission Electron Microscopy (HRTEM), X-ray Photoelectron Spectroscopy (XPS), Brunauer–Emmett–Teller (BET) and X-ray Diffraction (XRD).

2 Experimental

2.1 Production of carbon nanotubes (CNTs)

Carbon nanotubes were grown using the chemical vapour deposition (CVD) technique as well as a bimetallic (Fe–Co/$CaCO_3$) catalyst. The catalyst was prepared using Fe and Co metal salts supported on $CaCO_3$ by a wet impregnation method [22]. A Fe-Co precursor solution was prepared by adding 3.62 g of $Fe(NO_3)_3{\cdot}9H_2O$ and 2.47 g of $Co(NO_3)_2{\cdot}6H_2O$ into 50 ml distilled water. A mass of 10 g $CaCO_3$ was then added to the mixture and allowed to react for 60 min under constant stirring speed of 700 rpm until a gel was formed. The gel was allowed to dry at 120 °C for 12 h and then cooled to room temperature. After cooling, the granule solid was grounded and screened through a 150 µm sieve into a fine powder. The powder was calcined at a temperature of 400 °C for 16 h. A mass of 0.5 g of the bimetallic Fe-Co/$CaCO_3$ catalyst was spread to form a thin layer in a ceramic boat. The boat was then placed in a CCVD reactor. The reactor was first purged using argon gas at a flow rate of 30 ml min^{-1} for 90 min and then heated at a ramping rate of 10 °C min^{-1} until a temperature of 700 °C was reached. At 700 °C, the argon flow rate was adjusted to 190 ml min^{-1} and acetylene (as source of carbon) was introduced into the reactor at a flow rate of 290 ml min^{-1} for a period of 60 min and then discontinued. The argon flow rate was reduced to 30 ml min^{-1} to cool the reactor to room temperature. The ceramic boat was removed and weighed to determine the quantity of CNTs produced.

The as-produced CNTs was purified by an acid treatment technique to remove the residual Fe, Co, CaO, $CaCO_3$, amorphous carbon and other impurities. The process involved continuous stirring of 1 g CNTs with 100 ml mixture of 30% H_2SO_4 and 10% HNO_3 (3:1) for 3 h at 45 °C in a sonicator. The mixture was washed with distilled water until a pH of 7 was reached, after which the carbon nanotubes was dried in an oven at 120 °C for 12 h.

2.2 Preparation of Pt-MWCNT electrode

A mass of 1 g purified MWCNTs was placed in a 50 ml glass beaker, mixed with 30 ml of 5% polyethylene glycol (PEG) and then subjected to agitation in an ultrasonic bath at room temperature for 30 min. The mixture was magnetically stirred under reflux for 4 h at room temperature and 10 ml of 0.01 M K_2PtCl_4 solution was introduced into the mixture. The mixture was then stirred for a period of 150 min and then filtered. This procedure was repeated for other samples at different stirring times of 180, 210 and 240 min. The residue was air dried at room temperature overnight followed by annealing at 120 °C for 12 h. The samples were then heated at 300 °C for 16 h, pulverized and sieved using a 212 µm mesh. The filtrate collected was analysed to determine the absorbance of platinate salt at a specific platinum wavelength of 215 nm. Extrapolation of the Bears Lambert Law was used to estimate the concentration of platinum deposited on the CNTs. A known amount (0.5 g) of Pt-MWCNT was dispersed in 10 ml of Texanol (2,2,4-trimethyl-1,3-pentanediol monoisobutyrate) and 5 ml of Acrylic resins (Poly (methyl acrylate) (PMA). This was stirred continuously until a homogeneous mixture of the paste was obtained. The final paste was screen printed onto a FTO glass substrate to determine the conductivity.

2.3 Characterization techniques

The amount of Pt nanoparticles deposited on the CNTs was determined using a UV–VIS 1800 series (Shimadzu, Japan) spectrophotometer. The morphologies of the as-produced CNTs, purified CNTs and Pt-MWCNTs materials were examined with a Zeiss Auriga HRSEM under the following operation conditions: current 10 mA, voltage 5 kV, aperture 0.4 mm and working distance 4–10.4 mm. The microscope was operated at an electron accelerated voltage of

5 kV for imaging. A HRTEM Zeiss Auriga equipped with EDS was further used to determine the microstructure and elemental composition under the operational conditions of 54 µA emission current, 3950 V extraction voltage and a wavelength resolution of 0.24 nm. XPS analysis of the MWCNTs and Pt-MWCNTs were carried out with a PHI 5400 XPS spectrometer using a non-monochromatic Mg Kα X-ray source under the following measurement conditions: energy $hv = 1253.6$ eV, voltage = 15 kV, power = 200 W and hemispherical sector analyzer. The machine was calibrated for the Au 4f7/2 binding energy (BE) of 83.96 eV and the spectrometer was adjusted to measured Cu $2p_{3/2}$ at a position of 932.67 eV binding energy (BE). All spectra obtained were corrected using the aliphatic adventitious hydrocarbon C (1s) peak at 284.8 eV. The purified CNTs and Pt-MWCNTs nanocomposite were also analysed by XRD using a Bruker AXS D8 Advance with Cu-Kα radiation, 40 kV and 40 mA. The specific surface area and pore sizes were estimated by a nitrogen physisorption technique, employing Brunauer-Emmet-Teller (BET) (NOVA 4200e model). Nitrogen gas was used for degassing of the sample.

Cyclic voltammetry was carried out in a conventional air–tight three electrode cell using 0.5 M H_2SO_4 electrolyte at room temperature and a computer controlled potentiostats (663 VA Stand Metrohm). Platinum wire was used as counter electrode while Ag/AgCl saturated in a KCl salt bridge serve as the reference electrode and the working electrode was a 7 mm diameter glassy carbon.

3 Results and discussion

3.1 UV–VIS spectroscopy analysis

Table 1 shows the percentage of Pt deposited on the CNTs as a function of deposition time. It was noticed that the absorbance and concentration of the filtrate decreases with increasing deposition time while the concentration of Pt increases. The sample with deposition time 240 min. had the highest % concentration of Pt which suggests the existence of a linear relationship between the deposition time and concentration.

3.2 High resolution scanning electron microscopy (HRSEM) of As-produce and purified CNTs

Figure 1 shows the SEM images of the (a) as-produced and (b) purified CNTs, respectively. The HRSEM image in Fig. 1a exhibits a slight degree of entanglement of the CNTs with some bright spots, which corresponds to the residual metal particle from the catalysts used for the growth of CNTs. However, the purified CNTs images shown in Fig. 1b, exhibits a well-arranged and non-entangle tubular randomly oriented morphology. Some Iron/Cobalt particles remained unreactive due to a shortage of some production parameters such as low synthesis time and decomposition temperature resulting in the formation of amorphous impurities [23, 24]. The presences of such impurities did not affect the morphological arrangement of the as-produced CNTs and the tubular network matrix remained unchanged.

3.3 High resolution scanning electron microscopy (HRSEM) of Pt-MWCNTs

Figure 1(A150–A240) shows the HRSEM micrographs of the Pt-MWCNTs for different deposition times. Results indicate that the morphology of the samples changes from a tubular morphology to a rough, entangled and whitish surface due to deposition of platinum nanoparticles. The degree of roughness is more pronounced at longer deposition times and can be attributed to the presence of Pt nanoparticles on the surface. The average diameter of the samples was measured using image-j software and the results obtained as 23 nm, 41 nm, 55 nm and 73 nm for the A150, A180, A210 and A240 samples, respectively, which also shows that the diameter of the nanocomposites increases with an increase in the amount of platinum deposited. Furthermore, it was noticed that the brightness of the tubes increased and this was ascribed to the homogeneous deposition of platinum nanoparticles on the MWCNTs. However, beyond the optimum deposition time of 240 min, surface of the nanotubes became more agglomerated. Similar trend was reported by Padmavathi et al. [20] who functionalized MWCNTs with platinum using ultrasonication method.

Table 1 UV–VIS analysis showing Pt percentage concentration on the CNTs

Deposition time (min)	Absorbance of filtrate (a.u.)	Filtrate concentration (g cm^{-3})	Concentration of Pt on CNTs (g cm^{-3})	% Concentration of Pt on CNTs
150	0.722	2.79	1.38	33.12
180	0.708	2.72	1.44	34.62
210	0.689	2.64	1.53	36.64
240	0.665	2.53	1.63	39.20

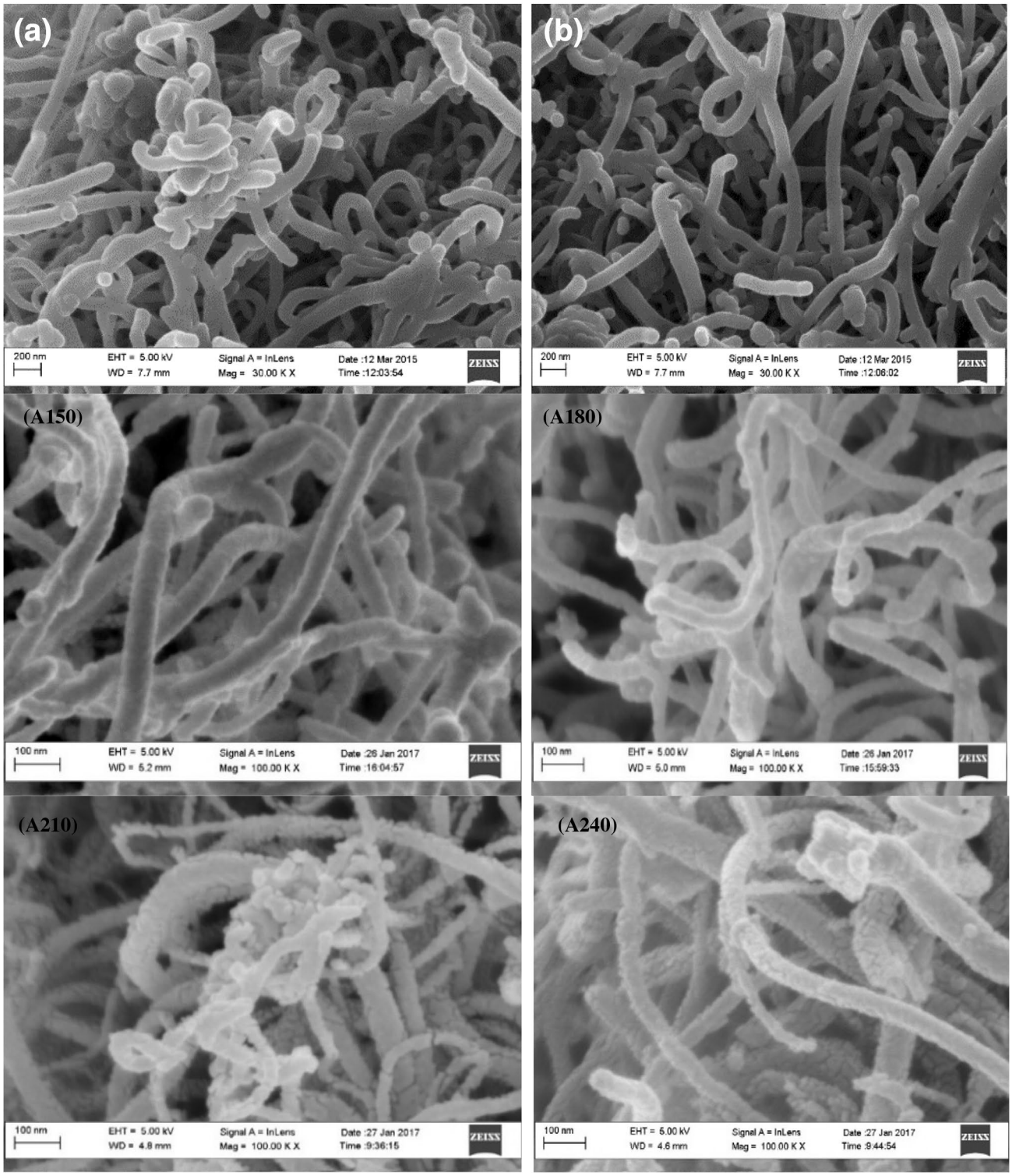

Fig. 1 HRSEM images of **a** As-produced MWCNTs; **b** Purified MWCNTs; (A150) Pt-deposited MWCNTs for 150 min; (A180) Pt-deposited MWCNTs for 180 min; (A210) Pt-deposited MWCNTs for 210 min; (A240) Pt-deposited MWCNTs for 240 min

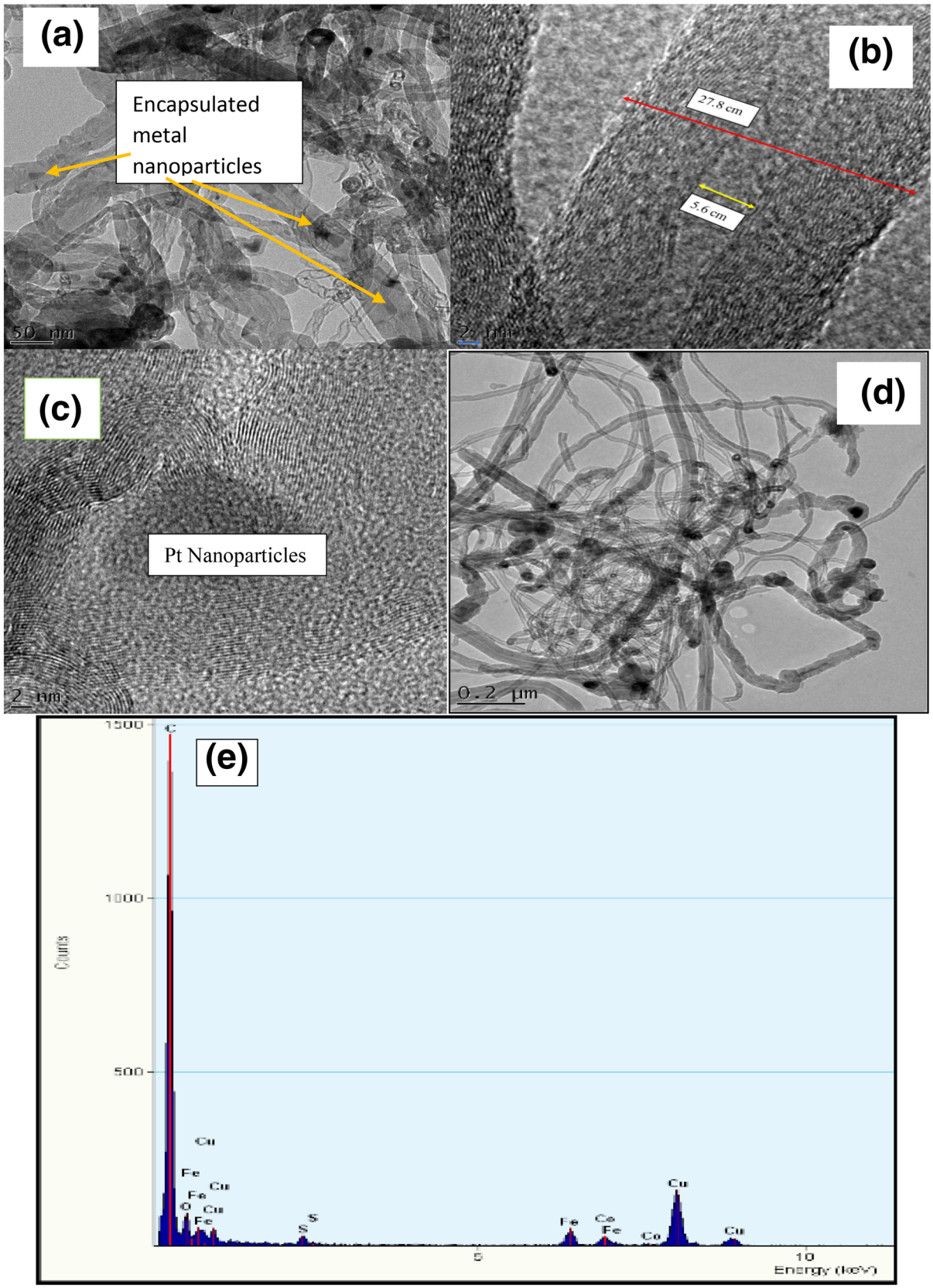

Fig. 2 HRTEM images of **a** Purified MWCNTs; **b** Pt-MWCNT; **c** high magnification Pt-MWCNTs, confirming the presence of Pt nanoparticles; **d** evidence of Pt nanoparticles evenly distributed on the outer surface of the tubes; **e** EDS spectra of Purified MWCNTs and **f** Pt-MWCNT confirming the presence of Pt

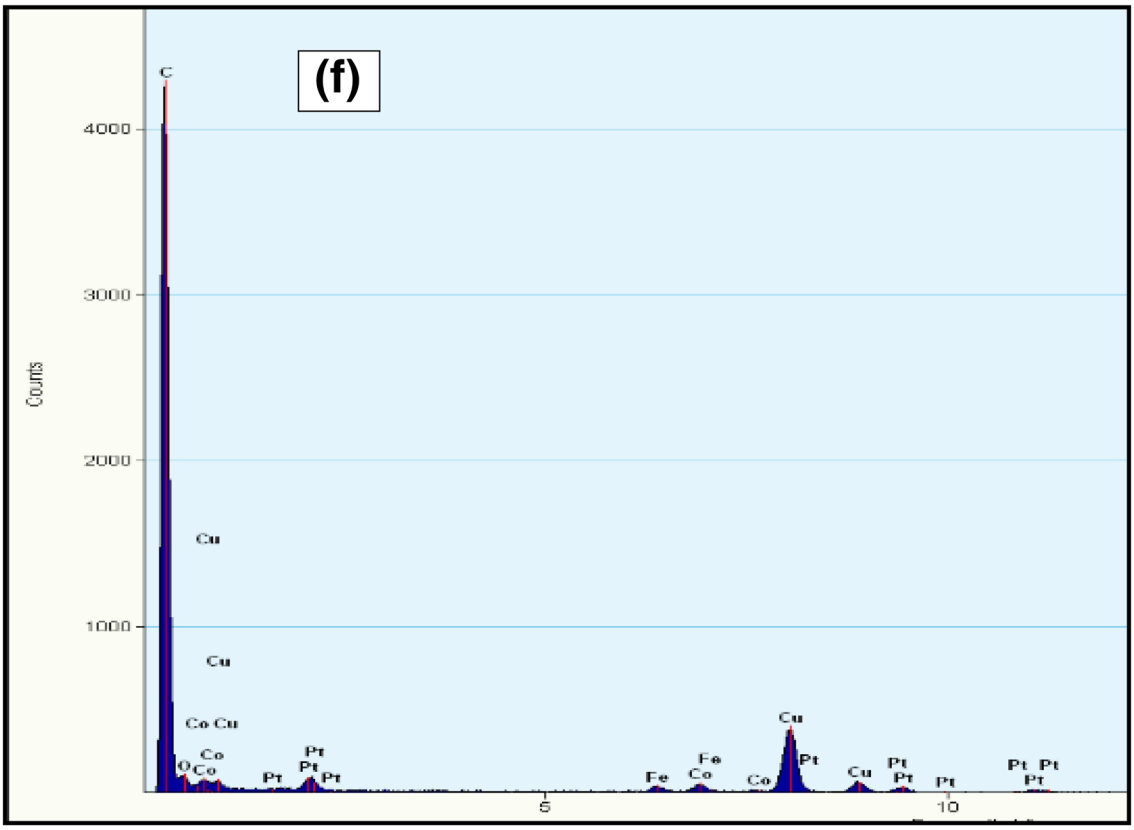

Fig. 2 (continued)

3.4 High resolution transmission electron microscope (HRTEM) of purified CNTs

Figure 2a shows a HRTEM image of the purified CNTs at high magnifications with encapsulated metal nanoparticles observed along the inner diameter of the tubes [25]. This shows that the acid purification step did not achieved complete removal of residual impurities. However, the XPS results confirmed most of these metallic impurities were entrapped within the inner and not outer layer of the tubes. Figure 2b depicts a HRTEM image of the purified CNT at low magnifications showing a multiwall nature with external and internal diameter 27.8 nm and 5.6 nm, respectively. The presence of lattice fringes further confirmed that the purified CNTs are highly crystalline with little or no defects.

3.5 High resolution transmission electron microscope (HRTEM) of Pt-MWCNTs

Figure 2c and d represents HRTEM images of Pt-MWCNTs at low and high magnifications. In Fig. 2c it is clear that the Pt particles were deposited on the surface of MWCNTs and image 2d shows that the particles are well–dispersed and homogeneously anchored on the surface of CNTs. The platinum particles were randomly distributed due to the hydrophobic nature of MWCNTs and not only that, the platinum particles were suppressed on the surface of MWCNTs. These ease of dispersion of Pt on the surface can be linked to the activation and functional groups on MWCNTs introduced during the acid purification step. The treatment of CNTs with a mixture of concentrated nitric and sulphuric acids did not only purify the carbon nanomaterials, it also resulted in the formation of carbonyl and hydroxyl groups which acted as anchoring sites and induced the impregnation of platinum nanoparticles [26–28]. This show a good agreement with the findings of Padmarathi et al. [20] who independently found that acid purification of MWCNTs aided ease dispersion of platinum nanoparticles,

3.6 Energy dispersive X-ray spectroscopy (EDS)

Figure 2e and f represent the elemental compositions of the purified and Pt-MWCNTs. In Fig. 2e the spectral revealed presence of Fe, Co, O Cu and S in addition to C as impurities. The fig clearly shows that despite the purification process these impurities were not totally removed. The observed Cu in the spectral is from the holey grid used during the analysis while sulphur and oxygen emanated from the H_2SO_4

used for purification. The Fe and Co signals confirm the presence of residual Fe/Co metal particles from the catalyst used in the synthesis. The EDS results in Fig. 2f revealed the presence of Pt in addition to C, O, Fe and Ca. The functionalization and purification of MWCNTs specifically influenced the dispersion and deposition of platinum particles.

3.7 X-ray photoelectron spectroscopy (XPS) of Pt-MWCNTs

Figure 3a shows two XPS survey spectra (1 and 2) of the purified CNTs and Pt-MWCNTs, respectively. The XPS scan confirmed C as the dominant species in the sample with binding energy 284.8 eV and atomic percentage of 74% and 69% for purified CNTs and Pt-MWCNTs, respectively. The element O was also detected at a binding energy of 532.5 eV and the Ca presence is the remnants of the catalyst support ($CaCO_3$) used in the production of the CNTs. High resolution XPS spectra for the C 1s peak is presented in Fig. 3b purified CNTs and (c) Pt-MWCNTs. Peak fits of the C energy envelope gave six individual groups as summarized in Table 2. The C 1s revealed a dominant single peak assigned to alkyl C and sp^2 hybridized graphite structure in CNTs corroborated the XRD result in Fig. 4. The table shows the calculated amount of graphitic and functional carbon atoms expressed in atomic % of the total carbon intensity. The decrease in carbon from 74 to 69% may be ascribed to the substitution by Pt atoms. The presence of Ar is attributed to Ar ion beam used for sputtering. Nonedetection of Fe and Co further corroborated HRTEM result, where the metallic particles were encapsulated in the inner layer of the CNTs.

The graphitic carbon peak position was normalized to a binding energy of 284.8 eV [29, 30]. The peaks at 287.7, 289.4 and 290.8 eV correspond to the formation of carbonyl and carboxyl groups during purification and

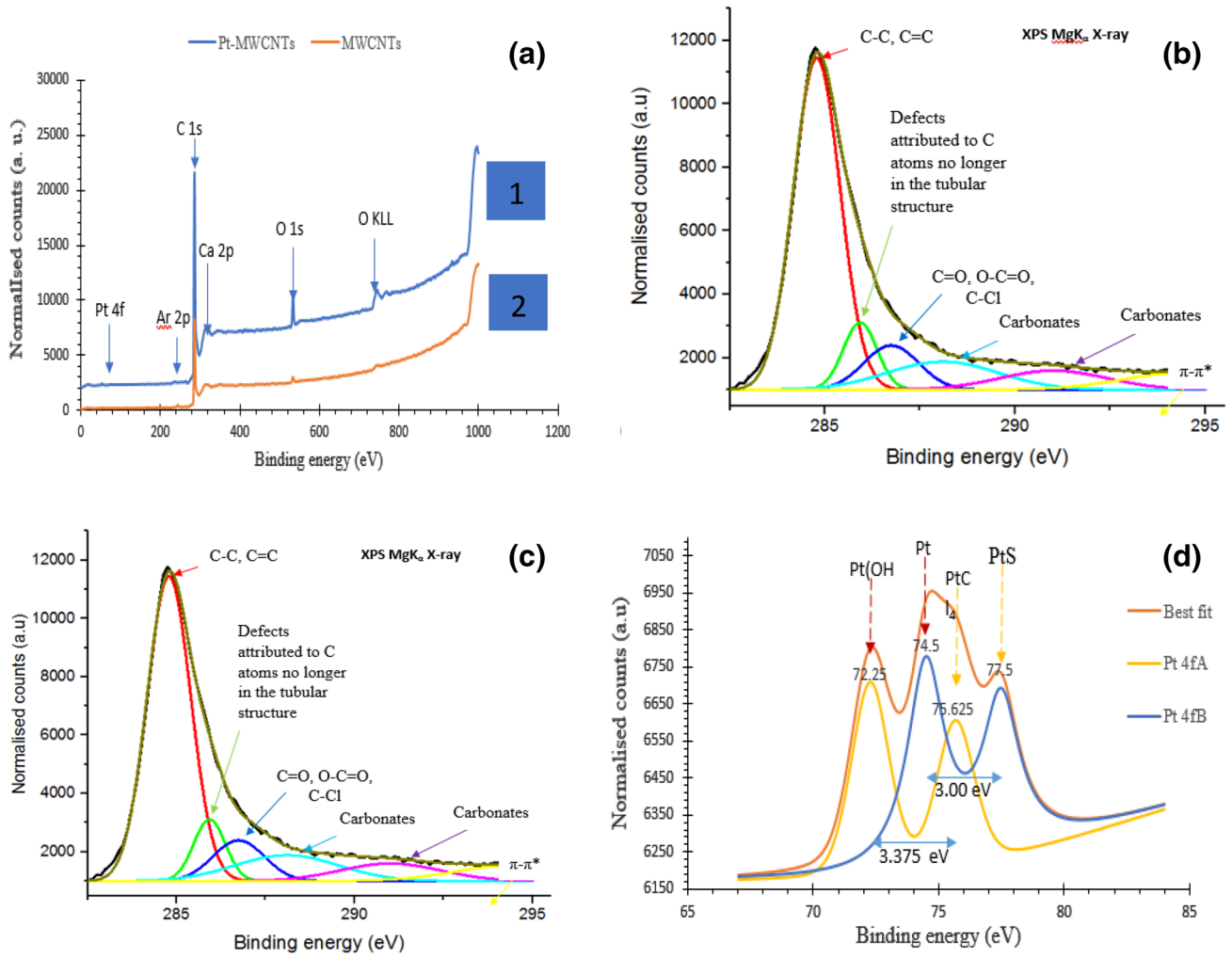

Fig. 3 XPS survey spectra of **a** purified (1) and Pt-MWCNTs (2) specimens; High resolution spectra of C 1 s for **b** purified MWCNTs and (c) Pt-MWCNTs and (d) high resolution spectrum of the Pt 4f region of the Pt-MWCNTs

Table 2 C(1 s) peak fitting results obtained for purified CNTs and Pt-MWCNTs

Binding Energy (eV)		FWHM (eV)		Area		C concentration (at%)		Chemical bound
Purified	Pt-MW	Purified	Pt-MW	Purified	Pt-MW	Purified	Pt-MW	
284.8	284.8	1.67	1.57	12,194	18,823	74	69	C–C, C=C
286.2	286.2	1.60	1.60	2232	4545	14	17	C–OH
287.7	287.7	1.60	1.60	1059	1944	6	7	C=O, O-C=O
289.4	289.4	1.60	1.60	604	1063	4	4	Carbonate
290.8	290.8	1.60	1.60	308	658	2	2	Carbonate
292.3	292.3	1.50	1.60	76	174	0	1	π-π*
Total				16,473	27,207	100	100	

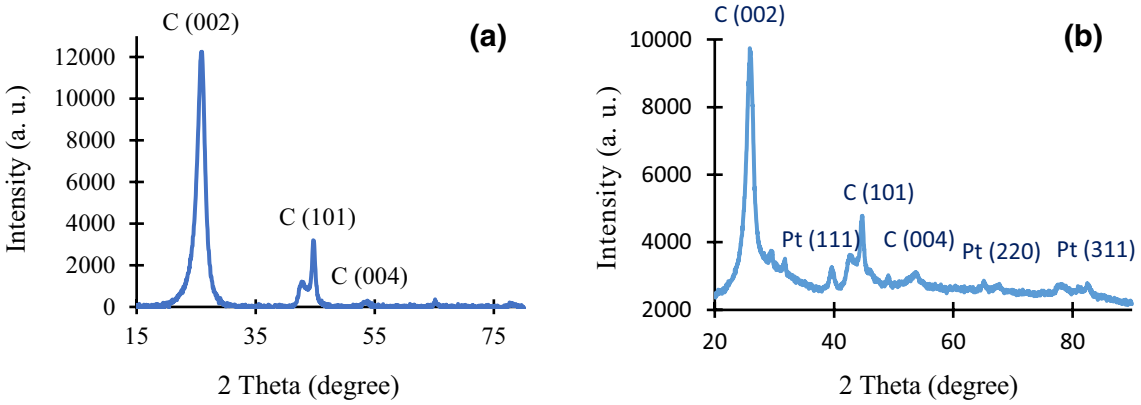

Fig. 4 XRD pattern of **a** purified MWCNTs and **b** Pt–MWCNT catalyst samples

functionalization. The presence of these functional groups confirmed the existence of strong intermolecular forces of attraction between the MWCNTs and Pt. Furthermore, the peak at 292.3 eV depicts a transition peak, which is assigned to π–π* and denote the chemical force of attraction on the surface of the CNTs. The peak observed at a binding energy of 286.21 eV accounted for defects on the nanotube structure due to the deposition of Pt [30–32]. The XPS peak fits in the Pt 4f energy region, as presented in Fig. 3d, show two different states of oxidation. The doublet peaks at 72.25 ($4f_{7/2}$) & 76.60 ($4f_{5/2}$) eV and 74.5 ($4f_{7/2}$) and 77.50 ($4f_{5/2}$) eV can be attributed to the functional group atoms attached to Pt during the functionalization processes to form the compounds $PtO/Pt(OH)_2$ and PtO_2. These functional groups [33, 34] originated from the acids (HNO_3 and H_2SO_4) used for purifications of the CNTs. The appearance of doublet peaks of platinum at the binding energies of 74.5 eV and 72.25 eV suggest the existence of platinum in the zero-oxidation state. The slight shift in the binding energies of Pt-MWCNTs compared to purified MWCNTs alone is an indication of electron transfer from the CNTs to platinum. Generally, CNTs is categorized as electron density rich materials, thus it is possible to conclude that the strong interaction between platinum particles and CNTs was due to electron transfer from CNTs to Platinum particles. The electronic transfer between CNTs and platinum promotes both catalytic activity and stability of the catalysts.

3.8 XRD analysis of Pt–MWCNT catalysts

The purified—and Pt-MWCNTs nanocomposites were investigated using XRD and the results are presented in Fig. 4a and b, respectively. The XRD pattern of the purified MWCNT sample revealed the characteristic pattern of graphitised carbon with crystal plane (002) as the major and intense diffraction peak at 2θ value of 25.98°. This corresponds to an inter-planar spacing of 0.3425 nm (3.43 Å). This value is slightly higher than that of ideal graphite (3.35 Å) resulting from expansion of the (002) planes in the CNT [35]. The sharp peaks pattern also indicates a high degree of crystallinity and suggests a low content of amorphous carbon and impurities [36]. Other peaks observed at 2θ values of 44.66° and 53.77°, with a corresponding crystal planes of (101) and (004) depict typical graphitic carbon (JSPDS 00-001-0646).

The XRD pattern of the Pt-MWCNTs nanocomposite (Fig. 4b) shows the characteristic graphitized carbon planes at indexes (002), (101) and (004) corresponding to

a face cantered cubic (fcc) structure while the crystalline platinum planes observed at 2θ values 39.60°, 67.83° and 82.45° were assigned to the planes (111), (220), and (311), respectively (JSPDS CARD no 00-01-0646), and this is in agreement with the work of Bharti and his group [21]. The C–C and C=C peaks obtained in the XPS analysis as shown in Table 2, corroborated the intense sharp diffraction peak at 2θ values of 26.98° displayed in Fig. 4a and b. Table 2 did not actually reveal the presence of Pt-O bond or Pt-C bond; however, XRD measurement confirmed the appearance of Pt at 2θ value of 39.60°, 67.83° and 82.45° with the crystal plane (111), (220) and (311). Also, there is no clear distinction in FWHM of both materials as indicated in Table 2 and Fig. 4, suggesting that the platinum did not penetrate the inner wall of the tubes but rather deposited on the outer layer of the CNTs. Comparatively, a decrease in the intensity of Pt-MWCNTs compared to purified MWCNTs attributable to the separation of layers caused by functionalization. Non-uniformity of the functionalization of MWCNTs with platinum may also be responsible for the low intensity of the peaks. Reduction in the intensity of peaks after functionalization either with acids or metals have been previously reported in the literature [37].

The average crystallite size of both purified and Pt-MWCNTs was calculated using the Debye–Scherrer formulae [38, 39] in Eq. (1) and Williamson-Hall [40, 41] in Eq. in (2)

$$D = \frac{K\lambda}{\beta \cos\theta} \tag{1}$$

$$\beta_{hkl} \cos\theta = \frac{K\lambda}{D} + 4\varepsilon \sin\theta \tag{2}$$

where D = the average crystalline size of the platinum particles (carbon nanotubes and platinum nanoparticles), K = the Scherrer constant = 0.94.

λ = the wavelength of X–ray radiation which is equal to 1.54051 Å, β = the full width at half-maximum (FWHM) of the {(002), (101), (004)} and {(111), (220), (311)} diffraction line for both purified and Pt-MWCNTs, respectively, θ = the Bragg angle measured in radians and ε is known as the strain broadening of the particles. This strain was assumed to be uniform in all crystallographic directions, thus considering the isotropic nature of the crystal, where the material properties are independent of the direction along which they are measured. A plot of 4sinθ along the x-axis and β_{hkl} cosθ along the y-axis gives a linear fit to the data, and the crystalline size was estimated from the y-intercept, and the strain ε, from the slope of the fit.

The crystallite size estimated from the diffraction peaks {C (002)} and {Pt (111)} were found to be 5.37 nm and 3.63 nm, using Scherrer equation and 9.28 nm and 3.18 nm for Williamson-Hall equation for purified MWCNTs and Pt-MWCNTs, respectively. Both methods show that the size of carbon nanotubes reduced upon the deposition of Pt. This reduction in size may be linked to the suppression of carbon intensity by the platinum based on ionic radius mechanism. The major diffraction peak for Pt was found to be Pt (111) at 2θ value of 39.60° with crystal size 3.63 nm. Figure 4b shows that the intensities of platinum peaks are very low compared to that of carbon. This indicates that the quantities of platinum in the nanocomposites is very low which in-turn reduced the cost of production of the electrode.

3.9 Brunauer–Emmett–Teller (BET) analysis of purified and Pt–CNT catalysts

The effect of platinum on the surface area and pore volume of the MWCNTs was investigated by the BET method and the results are shown in Table 3. It is obvious that the surface area and pore volume of the samples depend on the concentration of platinum nanoparticles deposited. The results further indicate that the surface area and pore volume increase with increase in the quantity of Pt nanoparticles on the surface. The literature [42] and [43] independently found that functionalization of CNTs with metals, influences the specific surface area of nanotubes. It causes the opening up of tube ends [44] and creates defects on the sidewalls of the nanotubes [45], in order to allow access into the cavity of the nanotubes. This implies that functionalization and deposition of platinum pushed the nanotubes away from each other given rise to higher surface area. Results presented indicate that the higher the concentration of the metal nanoparticles the higher the specific surface area. This result also agreed with the work of Padmavathi and his team [20] that says that specific surface area depends on reaction time of functionalization.

3.10 Electrochemical measurement of Pt-MWCNTs catalyst

Cyclic voltammetry is the most extensively used technique for acquiring qualitative information about electrochemical behaviour of the material. There are two ways to express the catalytic activities of the nanocomposites namely the

Table 3 BET analysis of Pt-MWCNTs catalyst samples

Pt concentration on MWCNTs	Surface area (m^2g^{-1})	Pore volume (cm^3g^{-1})
Purified	274.06	62.97
33.12 wt% Pt	432.6	19.14
34.62 wt% Pt	609.2	26.82
39.20 wt% Pt	858.7	38.82

mass activity and the specific activity [46]. The mass activity indicates the current per unit mass of composite which is important because the cost of the electrodes depends on the mass of Pt used. On the other hand, the specific activity which measures the unit surface area of nanocomposite shows the electrocatalytic activity of the Pt atoms on the surface [46, 47]. In this work, the CV plots in Fig. 5 represent the ordinate in microamperes per milligram of Pt. The different regions in Fig. 5a–d imply different processes taken place at the surface of the catalyst.

A maximum peak current density of 171.5 µA mg^{-1} Pt is obtained in the 39 wt% Pt–MWCNTs while the lowest current density, 68.25 µA mg^{-1} Pt was observed for the 33 wt% sample. Table 4 shows the peak current density (maximum current) and the corresponding voltage values for various loadings of Pt–CNTs catalysts as obtained from the cyclic voltammetry results in Fig. 5a–d. The region between − 0.25 and 0.35 depicts the desorption of the adsorbed platinum particles from the surface of Pt-MWCNTs. The region between 0.35 and 0.45 V represents the double layer charging and discharging, respectively. The tiny peak observed in Fig. 5b–d was due to increase in the loading of platinum and connotes oxidation of the surface oxide groups present in CNTs. It was also found that the intensity of the peak increased with increasing quantity of platinum nanoparticles. The regions beyond 0.75 V was attributed to the formation of C–OH bond on the surface of the catalyst, which further corroborates the XPS result.

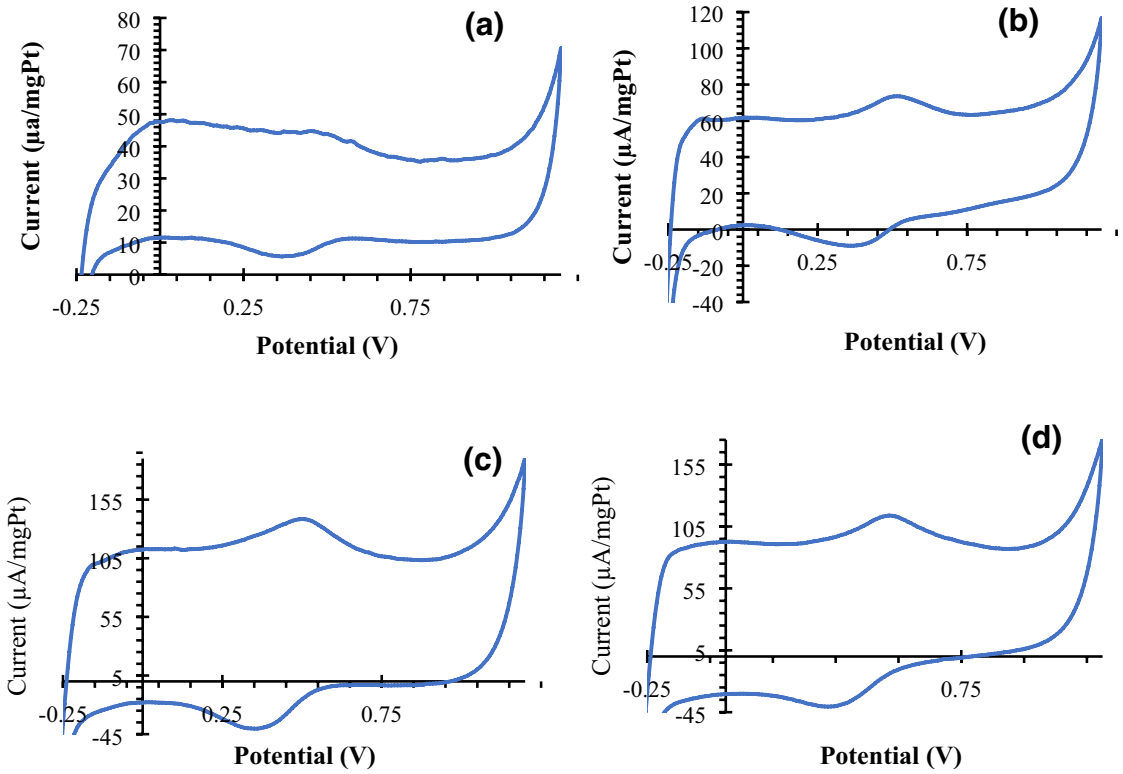

Fig. 5 Cyclic voltammograms of **a** 33 wt%, **b** 35 wt%, **c** 37 wt% and **d** 39 wt% Pt-MWCNT catalysts at a scan rate of 20 mV/s in nitrogen saturated 0.5 M H_2SO_4

Table 4 Electrocatalytic activity of Pt–MWCNTs catalysts

Catalyst loading (Pt-MWCNTs) (wt%)	Maximum current (µA.mg^{-1}Pt)	Minimum current (µA.mg^{-1}Pt)	Maximum voltage (V)	Minimum voltage (V)
33	68.25	5.772	1.195	0.375
35	113.7	− 8.911	1.195	0.360
37	185.7	− 40.39	1.195	0.345
39	171.5	− 40.22	1.195	0.310

3.11 Electrical conductivity of nanocomposite electrode

The electrical conductivity of the Pt-MWCNT nanocomposite film, deposited on a glass substrate as electrode, was determined from the relation given in Eq. (3) [48, 49].

$$\rho = R\frac{A}{L} \tag{3}$$

where $L = (0.839 \times 10^{-2}\text{cm})$, width, $W = (1.154 \times 10^{-2}\text{cm})$ and thickness = 0.011 cm. The resistivity, ρ of the film was estimated to be: $\rho = 2.0280 \times 10^{-4}\Omega\text{m}$ and conductivity σ: $\sigma = \frac{1}{\rho} = 4.927 \times 10^{3}\text{S/m}$.

The conductivity obtained was between that of pure Pt [50] and that of carbon graphite (CNTs) [51].

4 Conclusion

MWCNTs were synthesized via catalytic chemical vapour deposition technique and different concentrations of Pt were deposited on the synthesized MWCNTs by a wet impregnation method. The nanocomposites produced were characterized and high resolution scanning electron microscopy and high resolution transmission electron microscopy (HRSEM/HRTEM) confirmed that CNTs produced were Multi-walled in nature. EDS, XPS and XRD analysis confirmed successful deposition of Pt on the surface of CNTs. UV- vis spectroscopy confirmed that the amount of Pt deposited on CNTs increases with time, with the optimum percentage concentration obtained as 39.2 which corroborated XPS results. CV result also give maximum current density peak at 39 wt% Pt-MWCNTs and the least current density was obtained at 33 wt% Pt-MWCNTs. BET also confirmed that surface area is directly proportional to the amount of Pt deposited on the CNTs surface and deposition time under the applied conditions. The electrical conductivity of nanocomposites electrode produced was estimated to be $4.927 \times 10^{3}\ \text{Sm}^{-1}$ $4.927 \times 10^{3}\ \frac{\text{S}}{\text{m}}$ at room temperature, and this shows that the nanocomposite produced is highly conductive and considered as good material for solar cell counter electrode application.

References

1. S. Tsang, Y. Chen, P. Harris, M. Green, A simple chemical method of opening and filling carbon nanotubes. Nature **372**, 159 (1994)
2. A.S. Afolabi, A.S. Abdulkareem, A.D. Mhlanga, S.E. Iyuke, Synthesis and purification of bimetallic catalysed carbon nanotubes in a horizontal CVD reactor. J. Exp. Nanosci. **6**(3), 248–262 (2011)
3. S.A. Ijima, Growth model for carbon nanotubes. Phys. Rev. Lett. **69**(21), 3100–3103 (1992)
4. C. Liu, H.T. Cong, F. Li, P.H. Tan, H.M. Cheng, K. Lu, B.L. Zhou, Semi-continuous synthesis of single-walled carbon nanotubes by a hydrogen arc discharge method. Carbon **37**(11), 1865–1868 (1999)
5. H. Zhu, B. Jiang, C. Xu, D. Wu, Synthesis of high quality single walled carbon nanotube silks by the arc discharge technique. J. Phys. Chem. B **107**(27), 6514–6518 (2003)
6. H. Li, L. Guan, Z. Shi, Z. Gu, Direct synthesis of high purity single walled carbon nanotube fibers by arc discharge. J. Phys. Chem. B **108**(15), 4573–4575 (2004)
7. A. Thess, R. Lee, P. Nikolaev, H. Dai, P. Petit, J. Robert, C. Xu, Y.H. Lee, S.G. Kim, A.G. Rinzler, D.T. Colbert, Crystalline rope of metallic carbon nanotubes. Science **273**, 483–487 (1996)
8. N. Braidy, M.A. El-Khakani, G.A. Botton, Carbon nano-tubular structures synthesis by means of ultraviolet laser ablation. J. Mater. Res. **17**(9), 2189–2192 (2002)
9. R.L. Vanderwal, G.M. Berger, T.M. Ticich, Carbon nanotube synthesis in a flame using laser ablation for in situ catalyst generation. Appl. Phys. A **77**(7), 885–889 (2003)
10. H.H. Richter, Formation of nanotubes in low pressure hydrocarbon flames. Carbon **34**(3), 427–429 (1996). https://doi.org/10.1016/0008-6223(96)87612-3
11. R.L. Vander Wal, Optimization of flame synthesis for carbon nanotubes using supported catalyst. J. Phys. Chem. B **106**(51), 13122–13132 (2002)
12. T.T. Kyotani, Preparation of ultrafine carbon tubes in nanochannels of an anodic aluminum oxide film. Chem. Mater. Mater. **8**(8), 2109–2113 (1996). https://doi.org/10.1021/cm960063
13. Y. Yibo, M. Jianwei, Y. Zhihong, X. Fang-Xing, B.Y. Hong, L. Bin, Y. Yanhui, Carbon nanotube catalysts: recent advances in synthesis, characterization and applications. Chem. Soc. Rev. **44**, 3295 (2015). https://doi.org/10.1039/c4cs00492b
14. M.J. Yacaman, M.M. Yoshida, L. Rendon, J.G. Santiesteban, Catalytic growth of carbon microtubules with fullerene structure. Appl. Phys. Lett. **62**, 202–204 (1993)
15. S. Chaisitsak, A. Yamada, M. Konagai, Hot filament enhanced CVD synthesis of carbon nanotubes by using a carbon filament. Diam. Relat. Mater. **13**(3), 438–444 (2004)
16. A. Aliyu, A.S. Abdulkareem, A.S. Kovo, O.K. Abubakre, J.T. Tijani, I. Kariim, Synthesize multi-walled carbon nanotubes via catalytic chemical vapour deposition method on Fe-Ni bimetallic catalyst supported on kaolin. Carbon Lett. **21**, 33–50 (2017)
17. N. Rajalakshim, K.S. Dhathathreyan, Catalyst layer in PEMFC electrodes fabrication, characterization and analysis. Chem. Eng. J. **129**, 31–40 (2007)
18. M. Pawlyta, D. Łukowiec, A.D. Dobrzańska-Danikiewicz, Characterisation of carbon nanotubes decorated with platinum nanoparticles. J. Acheivement Mater. Manuf. Eng. **53**(2), 67–75 (2012)
19. C. Yu-Chun, L. Chia-Chun, C. Chun-Ping, Characterisation of platinum nanoparticles deposited on functionalised graphene sheets. Materials **8**, 6484–6497 (2015)
20. R. Padmavathi, A.D. Sandhya, N. Saranya, N. Gnanasundaram, D. Sangeetha, Synthesis and characterization of Pt supported on multiwalled carbon nanotubes for improved catalytic performance in fuel cell applications. J. Porous Mater. **22**, 647–658 (2015). https://doi.org/10.1007/s10934-015-9937-5
21. A. Bharti, G. Cheruvally, S. Muliankeezhu, Microwave assisted, facile synthesis of Pt/CNT catalyst for proton exchange membrane fuel cell application. Int. J. Hydrog. Energy (2017). https://doi.org/10.1016/j.ijhydene.2017.02.109
22. S. Banerjee, T. Hemraj, S. Wong, Covalent surface chemistry of single-walled carbon nanotubes. Adv. Mater. **1**, 17 (2005)
23. V. Datsyuk, C. Guerret-Piecourt, S. Dagreou, L. Billon, J.C. Dupin, E. Flahaut, Double walled carbon nanotube/polymer

composites via in situ nitroxide mediated polymerisation of amphiphilic block copolymers. Carbon **43**, 873–876 (2005)
24. A.S. Afolabi, Development of carbon nanotubes platinum electro catalytic electrodes for proton exchange membrane fuel cell., Faculty of Engineering and the Built Environment, University of the Witwatersrand., Johannesburg (2009)
25. C.P. Deck, G.S.B. McKee, K.S. Vecchio, Synthesis optimization and characterization of multiwalled carbon nanotubes. J. Electron. Mater. **35**, 211–223 (2006). https://doi.org/10.1007/BF02692438
26. Y. Zhou, F. Pervin, V.K. Rangari, S. Jeelani, Fabrication and evaluation of carbon nano fiber filled. carbon/epoxy composite. Mater. Sci. Eng. A **426**, 221–228 (2006)
27. Z. Chen, K.P. Bachmann, D. den Engelsen, I. Koehler, U.D. Wiechert, "Fabrication and characterization of carbon nanotube arrays using sandwich catalyst stacks. Carbon **44**, 225–230 (2006)
28. X. Yang, T. Zou, C. Shi, E. Lie, C. He, N. Zhao, Effect of carbon nanotube content on the properties of in-situ synthesis CNT reinforced Al composites. Mater. Sci. Eng. A. **660**, 11 (2016)
29. N. Zhang, J. Xie, V. Varadan, Functionalization of carbon nanotubes by potassium permanganate assisted with phase transfer catalyst. Smart Mater. Struct. **11**, 962–965 (2002)
30. D.J. Haung, C.M. Yeh, M.Y. Chen, J. Hwang, C.S. Kou, Field emission from a carbon nanofiber/carbon nanocone composite structure fabricated by a two-step growth process. J. Electrochem. Soc. **153**, H15–H17 (2006)
31. O.P. Hugh, *Handbook of Carbon, Graphite, Diamond, and Fullerenes: Properties, Processing, and Applications* (Noyes Publications, Park Ridge, 1993), p. 61
32. M.V. Naseh, A.A. Khodadadi, Y. Mortazavi, O.A. Sahraei, F. Pourfayaz, S.M. Sedghi, Functionalization of carbon nanotubes using nitric acid oxidation and DBD plasma. Int. J. Chem. Mol. Nucl. Mater. Metall. Eng. **3**(1), 33–35 (2009)
33. S. Iijima, Helical microtubules of graphitic carbon. Nature **354**, 56 (1991)
34. F.M. John, F.S. William, E.S. Peter, D.B. Kenneth, *Handbook of X-ray Photoelectron Spectroscopy: A Reference Book of Standard Spectra for Identification and Interpretation of XPS Data* (Perkin-Elmer Corporation Physical Electronics Div, Eden Prairie, 1992)
35. E. Gharibshahi, E. Saion, Influence of dose on particle size and optical properties of colloidal platinum nanoparticles. Int. J. Mol. Sci. **13**, 14723–14741 (2012)
36. J. Xie, S. Wang, L. Aryasomayajula, V.K. Varadan, Platinum decorated carbon nanotubes for highly sensitive amperometric glucose sensing. Nanotechnology **18**(6), 065503 (2007)
37. G. Ovejero, J.L. Sotelo, M.D. Romero, A. Rodrıguez, M.A. Ocana, G. Rodrıguez, J. Garcıa, Multiwalled carbon nanotubes for liquid-phase oxidation. Functionalization, characterization, and catalytic activity. Ind. Eng. Chem. Res. **45**, 2206–2212 (2006)
38. A.L. Patterson, The Scherrer formula for I-ray particle size determination. Phys. Rev. **56**, 1 (1993)
39. C. Coutanceau, S. Baranton, T.W. Napporn, Platinum Fuel Cell Nanoparticle Syntheses: effect on morphology, structure and electrocatalytic behavior, in *The Delivery of Nanoparticles*, ed. by A.A. Hashim (InTech, Rijeka, 2012)
40. Y. Slimania, M.A. Almessiere, E. Hannachi, A. Baykal, A. Manikandan, M. Mumtaz, F.B. Azzouz, Influence of WO_3 nanowires on structural, morphological and flux pinning ability of YBa_2Cu_3Oy superconductor. Ceram. Int. (2018). https://doi.org/10.1016/j.ceramint.2018.10.201
41. S. Mustapha, M.M. Ndamitso, A.S. Abdulkareem, J.O. Tijani, D.T. Shuaib, A.K. Mohammed, A. Sumaila, Comparative study of crystallite size using Williamson-Hall and Debye-Scherrer plots for ZnO nanoparticles. Adv. Nat. Sci. **10**, 045013 (2019)
42. E.M. Birch, T.A. Ruda-Eberenz, M. Chai, R. Andrews, R.L. Hatfield, Properties that influence the specific surface areas of carbon nanotubes and nanofibers. Ann. Occupat. Hyg. **57**(9), 1148–1166 (2013)
43. W. Zhang, E. Croiset, P.L. Douglas, M.W. Fowler, E. Entchev, Simulation of a tubular solid oxide fuel cell stack using Aspen Plus TM unit operation models. Energy Convers. Manag. **46**, 181–196 (2005)
44. S. Sharma, B.G. Pollet, Support materials for PEMFC and DMFC electro catalysts: a review. J. Power Sour. **208**, 96–119 (2012)
45. A.S. Abdulkareem, B. Suleiman, A.T. Abdulazeez, I. Kariim, O.K. Abubakre, A.S. Afolabi, Synthesis and characterisation of carbon nanotubes on Fe/Al_2O_3 composite catalyst by chemical vapour deposition method, in *Proceedings of the World Congress on Engineering and Computer Science, San Francisco, USA, 11*. Retrieved February 2017. -4, p. 11 (2016)
46. L.A. Dobrzański, M. Pawlyta, A. Krzton, B. Liszka, K. Labisz, Synthesis and characterization of carbon nanotubes decorated with platinum nanoparticles. J. Acheivement Mater. Manuf. Eng. **39**(2), 184–189 (2010)
47. H.F. Aritonang, D. Onggo, C. Ciptati, C.I. Radiman, Synthesis of platinum nanoparticles from K2PtCl4 solution using bacterial cellulose matrix. J. Nanopart. **2014**, 1–6 (2014)
48. K.A. Charles, N.O.S. Mathew, *Fundamentals of Electric Circuits*, 2nd edn. (McGraw-Hill, New York, 2004), p. 30
49. R.R. Christopher, *Fundamental Electrical and Electronic Principles*, 3rd edn. (Elsevier, Amsterdam, 2008), p. 21
50. H. Ago, T. Kugler, F. Cacialli, W. Salaneck, M. Shaffer, A. Windle, R. Friend, Work functions and surface functional groups of multiwall carbon nanotubes. J. Phys. Chem. B **103**, 8116–8121 (1999)
51. National Institute of Standards and Technology (NIST), X-ray Photoelectron Spectroscopy Standard Reference Database 20, Version 4.1," NIST (2017)